

Graphical Abstract

Real-time Attitude Control of a Quadrotor Platform using a Linear Quadratic Integral Differential Game Approach

Hadi Nobahari, Ali BaniAsad, Reza Pordal, Alireza Sharifi

Real-time Attitude Control of a Quadrotor Platform using a Linear Quadratic Integral Differential Game Approach

Hadi Nobahari, Ali BaniAsad, Reza Pordal, Alireza Sharifi

^a*Department of Aerospace Engineering Sharif University of Technology, Tehran, Iran*

Abstract

In this study, a linear quadratic integral differential game approach is applied to regulate and track the attitude angle of an experimental platform of the quadrotor using two players. One produces commands for each channel of the quadrotor and another creates the worst disturbance by minimizing a quadratic criterion with integral action. For this purpose, first, the attitude dynamics of the platform are modeled and its parameter is identified based on the Nonlinear Least Squares Trust-Region Reflective method. The performance of the proposed controller is evaluated for regulation and tracking problems. The ability of the controller is examined in the disturbance rejection. Moreover, the influence of uncertainty modeling is studied on the obtained results. Then, the performance of the proposed controller is compared with the classic PID, Linear Quadratic Regulator, and Linear Quadratic Integral Regulator. The result demonstrates the effectiveness of the Game Theory on the Linear Quadratic Regulator approach when the input disturbance occurs.

Keywords:

Linear Quadratic controller, Differential Game Theory, Quadrotor, Continuous State-space Model, three-degree-of-freedom Experimental Platform, Attitude Control Optimization, Robust Disturbance Rejection.

Email addresses: nobahari@sharif.edu (Hadi Nobahari),
ali.baniasad@ae.sharif.edu (Ali BaniAsad), email address (Reza Pordal),
ar.sharifi@sharif.edu (Alireza Sharifi)

1. Introduction

In this paper, an LQIR method, called LQIR-DG controller is suggested to produce the optimal and robust control command, i.e. rotational velocity command using the game theory approach. Since the LQIR-DG controller is affected by an exact model of the plant, the quadrotor's experimental platform is modeled and its parameters are identified based on experimental data. For control purposes, its linear state-space form is extracted using linearization of the nonlinear UAV model. Then, the LQIR-DG technique is applied in real-time to the experimental platform. The performance of the LQIR-DG method is evaluated in the presence of the disturbance and modeling error for regulation and tracking purposes. A comparison is also performed between the results of the classical PID, LQR, and LQIR and the proposed approach in real-time mode. The results show the proposed control structure is effective in the control of the quadrotor platform.

This research is organized as follows: section 2 presents the problem statement. In section 3, the dynamic platform is modeled. Then, the presented controller architecture is denoted in section 4. In sections 5 and 6, numerical results and a conclusion are represented, respectively.

2. Problem Statement

The experimental quadrotor platform rotates freely with rotational velocity about its roll, pitch, and yaw axes, according to Figure 1. The Euler angles (ϕ, θ, ψ) and the angular velocities in the body frame (p, q, r) are measured using an Attitude Heading Reference System (AHRS). The measured states are utilized in the structure of the proposed controller to stabilize the quadrotor platform. The graphical abstract of the proposed controller structure is depicted in Figure 2.



Figure 1: 3DoF Platform of the Quadrotor.

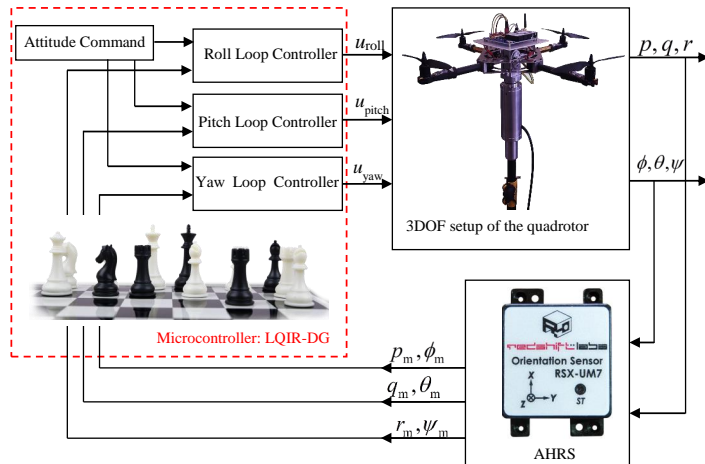


Figure 2: Graphical Abstract of the LQIR-DG Controller

3. Dynamic Model of the Quadrotor Platform

Here, the nonlinear model for the quadrotor platform is presented. Then, a state-space model and a linear model are developed for control purposes to be utilized in the controller strategy. Finally, a nonlinear identification method is applied to identify the parameters of the quadrotor.

3.1. Quadrotor Configuration

According to Figure 3, the 3DoF quadrotor schematic is including four rotors rotating the z_B axis in the body frame with a rotational velocity ω . To eliminate the yawing moment, rotors (2, 4) and (1, 3) rotate clockwise and counter clockwise, respectively.

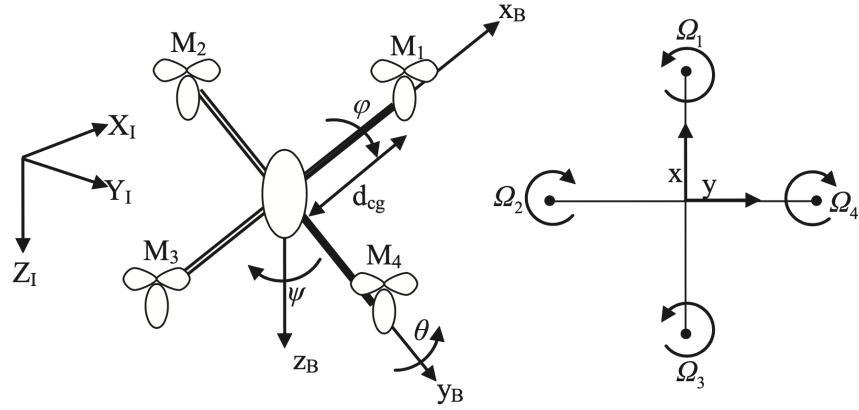


Figure 3: Quadrotor Configuration.

3.2. Dynamic Modeling of the Quadrotor Platform

Here, according to Newton-Euler, the model of the quadrotor platform is presented as follows (Bouabdallah and Siegwart, 2007; Bouabdallah, 2007):

$$\dot{p} = \frac{I_{yy} - I_{zz}}{I_{xx}} qr + q \frac{I_{rotor}}{I_{xx}} \Omega_r + \frac{b d_{cg} (\Omega_{c,2}^2 - \Omega_{c,4}^2)}{I_{xx}} + \frac{d_{roll}}{I_{xx}} \quad (1)$$

$$\dot{q} = \frac{I_{zz} - I_{xx}}{I_{yy}} rp + p \frac{I_{rotor}}{I_{xx}} \Omega_r + \frac{b d_{cg} (\Omega_{c,1}^2 - \Omega_{c,3}^2)}{I_{yy}} + \frac{d_{pitch}}{I_{yy}} \quad (2)$$

$$\dot{r} = \frac{I_{xx} - I_{yy}}{I_{zz}} pq + \frac{d (\Omega_{c,1}^2 - \Omega_{c,2}^2 + \Omega_{c,3}^2 - \Omega_{c,4}^2)}{I_{zz}} + \frac{d_{yaw}}{I_{zz}} \quad (3)$$

where $\Omega_{c,i}$ ($i = 1, 2, 3, 4$) is the rotational velocity computed as:

$$\Omega_{c,1}^2 = \Omega_{\text{mean}}^2 + \frac{1}{2b d_{\text{cg}}} u_{\text{pitch}} + \frac{1}{4d} u_{\text{yaw}} \quad (4)$$

$$\Omega_{c,2}^2 = \Omega_{\text{mean}}^2 + \frac{1}{2b d_{\text{cg}}} u_{\text{roll}} - \frac{1}{4d} u_{\text{yaw}} \quad (5)$$

$$\Omega_{c,3}^2 = \Omega_{\text{mean}}^2 - \frac{1}{2b d_{\text{cg}}} u_{\text{pitch}} + \frac{1}{4d} u_{\text{yaw}} \quad (6)$$

$$\Omega_{c,4}^2 = \Omega_{\text{mean}}^2 - \frac{1}{2b d_{\text{cg}}} u_{\text{roll}} - \frac{1}{4d} u_{\text{yaw}} \quad (7)$$

Ω_{mean} is rotational velocity of the rotors. Also, d_{cg} , d , and b represent the distance between the rotors and the gravity center, drag factor, and thrust factor, respectively. d_{roll} , d_{pitch} , and d_{yaw} denote the disturbances produced in the body coordinate frame. Additionally, I_{xx} , I_{yy} , and I_{zz} are the moments of inertia, and I_{rotor} is the rotor inertia about its axis. Euler angle rates are also determined from angular body rates as follows:

$$\begin{bmatrix} \dot{\phi} \\ \dot{\theta} \\ \dot{\psi} \end{bmatrix} = \begin{bmatrix} 1 & \sin(\phi) \tan(\theta) & \cos(\phi) \tan(\theta) \\ 0 & \cos(\phi) & -\sin(\phi) \\ 0 & \sin(\phi)/\cos(\theta) & \cos(\phi)/\cos(\theta) \end{bmatrix} \begin{bmatrix} p \\ q \\ r \end{bmatrix} \quad (8)$$

The residual rotor velocity, denoted by $\Omega_{c,r}$, is calculated as follows:

$$\Omega_{c,r} = -\Omega_{c,1} + \Omega_{c,2} - \Omega_{c,3} + \Omega_{c,4} \quad (9)$$

3.3. State-Space Formulation

By defining $x_1 = p$, $x_2 = \phi$, $x_3 = q$, $x_4 = \theta$, $x_5 = r$, and $x_6 = \psi$, the formulation of the quadrotor platform is presented as follows:

$$\dot{x}_1 = \Gamma_1 x_3 x_5 + \Gamma_2 x_3 \Omega_r + \Gamma_3 b d_{\text{cg}} (\Omega_{c,1}^2 - \Omega_{c,3}^2) + \Gamma_3 d_{\text{roll}} \quad (10)$$

$$\dot{x}_2 = x_1 + (x_3 \sin(x_2) + x_3 \cos(x_2)) \tan(x_4) \quad (11)$$

$$\dot{x}_3 = \Gamma_4 x_1 x_5 - \Gamma_5 x_1 \Omega_r + \Gamma_6 b d_{\text{cg}} (\Omega_{c,2}^2 - \Omega_{c,4}^2) + \Gamma_6 d_{\text{pitch}} \quad (12)$$

$$\dot{x}_4 = x_3 \cos(x_4) - x_5 \sin(x_2) \quad (13)$$

$$\dot{x}_5 = \Gamma_7 x_1 x_3 + \Gamma_8 d (\Omega_{c,1}^2 - \Omega_{c,2}^2 + \Omega_{c,3}^2 - \Omega_{c,4}^2) + \Gamma_8 d_{\text{yaw}} \quad (14)$$

$$\dot{x}_6 = (x_3 \sin(x_4) + x_5 \cos(x_2)) / \cos(x_4) \quad (15)$$

where $\Gamma_i (i = 1, \dots, 8)$ is defined as:

$$\begin{aligned}\Gamma_1 &= \frac{I_{yy} - I_{zz}}{I_{xx}}, & \Gamma_2 &= \frac{I_{rotor}}{I_{xx}}, & \Gamma_3 &= \frac{1}{I_{xx}} \\ \Gamma_4 &= \frac{I_{zz} - I_{xx}}{I_{yy}}, & \Gamma_5 &= \frac{I_{rotor}}{I_{yy}}, & \Gamma_6 &= \frac{1}{I_{yy}} \\ \Gamma_7 &= \frac{I_{xx} - I_{yy}}{I_{zz}}, & \Gamma_8 &= \frac{1}{I_{zz}}\end{aligned}\quad (16)$$

Moreover, the measurement vector, obtained from the AHRS is presented as follows:

$$\mathbf{z} = [p \ q \ r \ \phi \ \theta \ \psi]^T + \boldsymbol{\nu} \quad (17)$$

where $\boldsymbol{\nu}$ is a Gaussian white noise. Moreover, the superscripts T indicate the transpose notation.

3.4. Linear Model

By defining $\dot{\mathbf{x}} = [\dot{\mathbf{x}}_{roll} \ \dot{\mathbf{x}}_{pitch} \ \dot{\mathbf{x}}_{yaw}]^T$, the linear model of the quadrotor platform represented about the equilibrium points ($\mathbf{x}_e^* = 0$ and $\mathbf{u}_e^* = 0$) as:

$$\dot{\mathbf{x}}(t) = \mathbf{A} \mathbf{x}(t) + \mathbf{B}(t) (\mathbf{u}(t) + \mathbf{d}(t)) \quad (18)$$

Here $\mathbf{x}_{roll} = [p \ \phi]^T$, $\mathbf{x}_{pitch} = [q \ \theta]^T$, and $\mathbf{x}_{yaw} = [r \ \psi]^T$. \mathbf{A} is the dynamic system matrix, denoted as:

$$\mathbf{A} = \begin{bmatrix} \mathbf{A}_{roll} & \mathbf{0} & \mathbf{0} \\ \mathbf{0} & \mathbf{A}_{pitch} & \mathbf{0} \\ \mathbf{0} & \mathbf{0} & \mathbf{A}_{yaw} \end{bmatrix} \quad (19)$$

Here, $\mathbf{A}_{roll} = \mathbf{A}_{pitch} = \mathbf{A}_{yaw} = \begin{bmatrix} 0 & 0 \\ 1 & 0 \end{bmatrix}$. Also, \mathbf{B} is the input matrix defined as:

$$\mathbf{B} = \begin{bmatrix} \mathbf{B}_{roll} & \mathbf{0} & \mathbf{0} \\ \mathbf{0} & \mathbf{B}_{pitch} & \mathbf{0} \\ \mathbf{0} & \mathbf{0} & \mathbf{B}_{yaw} \end{bmatrix} \quad (20)$$

Here, $\mathbf{B}_{roll} = \begin{bmatrix} 1 \\ I_{xx} \end{bmatrix}^T$, $\mathbf{B}_{pitch} = \begin{bmatrix} 1 \\ I_{yy} \end{bmatrix}^T$, and $\mathbf{B}_{yaw} = \begin{bmatrix} 1 \\ I_{zz} \end{bmatrix}^T$.

3.5. Identification of the Platform Parameters

In this section, the Nonlinear Least Squares (NLS) algorithm is utilized for estimating the model parameters (Γ) of the 3DoF experimental platform using experimental data. This technique is based on the Trust-Region Reflective (TRR) method, which iteratively finds the values of the model parameters by minimizing a cost function, defined as:

$$\min_{\Gamma_i} (\| e(\Gamma_i) \|^2) = \min_{\Gamma_i} = \left(\sum (\mathbf{z}_j - \hat{\mathbf{z}}_j)(\mathbf{z}_j - \hat{\mathbf{z}}_j)^T \right) \quad (21)$$

where \mathbf{z} and $\hat{\mathbf{z}}$ are the experimental and simulated output signals, when the same input signals are applied ones. Moreover, j is the number of scenarios. To find a vector Γ , the optimization process performs until convergence is achieved. The structure of the identification approach is illustrate in figure 4

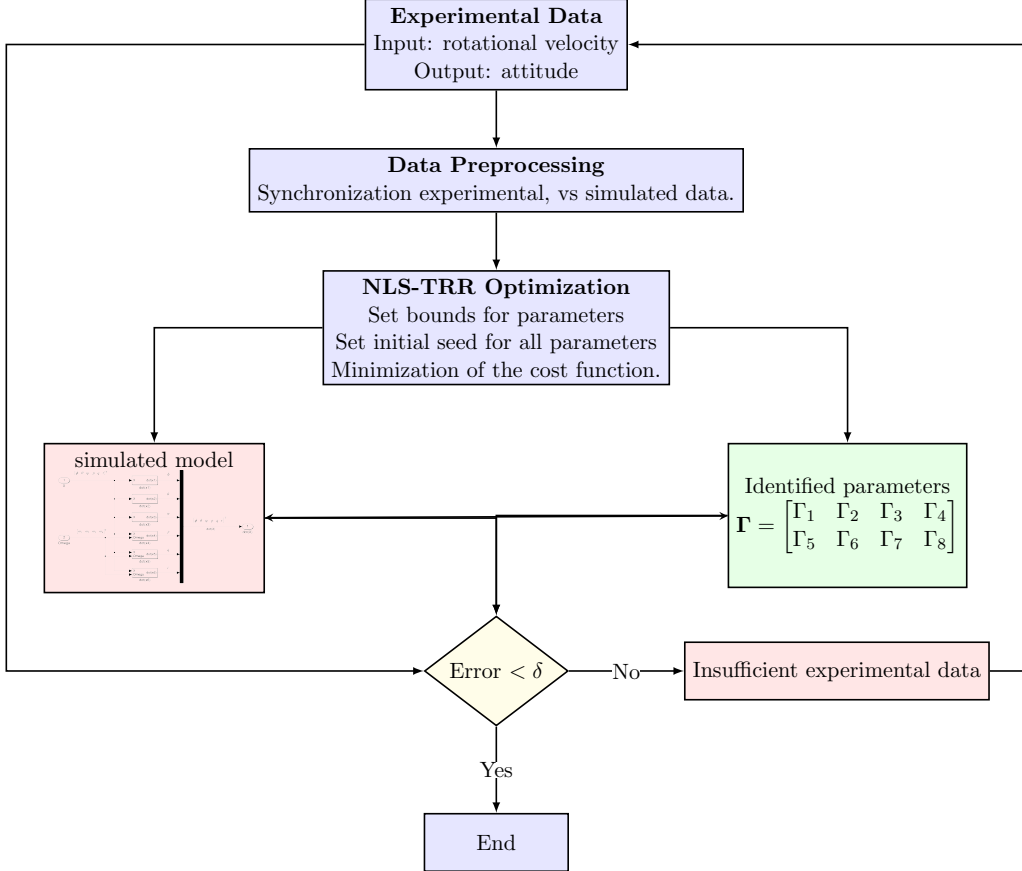


Figure 4: Structure of TRRLS identification approach.

4. Structure of the LQIR-DG Controller

Here, first, the augmented states of the quadrotor platform, including the states and their integrals are selected to utilize in the structure of the LQIR-DG controller for eliminating the steady states errors. Then, the design methodology of the LQR-DG controller is introduced to generate optimal control commands for the 3DoF quadrotor platform.

4.1. Augmented States

To augment an integral action into the control strategy architecture, the augmented states are defined as $\mathbf{x}_{\mathbf{a}_i} = \begin{bmatrix} \mathbf{x} & \int \mathbf{x} \end{bmatrix}^T$. Then, the model of the quadrotor platform, utilized in the controller structure, is presented as:

$$\dot{\mathbf{x}}_a(t) = \begin{bmatrix} \mathbf{A} & \mathbf{0} \\ \mathbf{I} & \mathbf{0} \end{bmatrix} \mathbf{x}_a(t) + \begin{bmatrix} \mathbf{B} \\ \mathbf{0} \end{bmatrix} (\mathbf{u}(t) + \mathbf{d}(t)) \quad (22)$$

$$\mathbf{A}_a = \begin{bmatrix} \mathbf{A} & \mathbf{0} \\ \mathbf{I} & \mathbf{0} \end{bmatrix} \quad (23)$$

where, the notation \mathbf{I} denotes the identity matrix.

4.2. LQIR-DG Control Scheme with Integral Action

In the proposed controller scheme, two fundamental players are selected in accordance with the game theory approach. The primary player determines the control commands, while another player generates the worst possible disturbance. To achieve the primary objective, first player minimizes the following cost function but the other player maximize it:

$$\min_u \max_d J(\mathbf{x}_{a_i}, d_i, u_i) = J(\mathbf{x}_{a_i}, u_i^*, d_i^*) = \min_d \max_u \int_0^{t_f} \left(\mathbf{x}_{a_i}^T \mathbf{Q}_i \mathbf{x}_{a_i} + u_i^T R u_i - d_i^T R_d d_i \right) dt \quad (24)$$

where t_f is stop time. \mathbf{Q}_i , R_d , and R are weight coefficients of the function. By solving the above problem, the control command is computed as follows (Engwerda, 2006):

$$u_i(t) = -\mathbf{K}_i(t) \mathbf{x}_{a_i}(t) \quad (25)$$

Moreover, the worst disturbance is obtained as:

$$d_i(t) = \mathbf{K}_{d_i}(t) \mathbf{x}_{a_i}(t) \quad (26)$$

Here, \mathbf{K}_{d_i} and \mathbf{K}_i are gain values defined as follows:

$$\mathbf{K}_{d_i} = R_d^{-1} \mathbf{B}_{a_{d_i}}^T \mathbf{P}_{a_{d_i}}(t) \quad (27)$$

$$\mathbf{K}_i = R^{-1} \mathbf{B}_{a_i}^T \mathbf{P}_{a_i}(t) \quad (28)$$

where $\mathbf{P}_{a_i}(t)$ and $\mathbf{P}_{a_{d_i}}(t)$ satisfy

$$-\mathbf{A}_a^T \mathbf{P}_{a_{d_i}}(t) - \mathbf{Q}_i - \mathbf{P}_{a_{d_i}}(t) \mathbf{A}_a + \mathbf{P}_{a_{d_i}}(t) \mathbf{S}_{a_i}(t) \mathbf{P}_{a_i}(t) + \mathbf{P}_{a_{d_i}}(t) \mathbf{S}_{a_{d_i}}(t) \mathbf{P}_{a_{d_i}}(t) = \mathbf{0} \quad (29)$$

$$-\mathbf{A}_a^T \mathbf{P}_{a_i}(t) - \mathbf{Q}_i - \mathbf{P}_{a_i}(t) \mathbf{A}_a + \mathbf{P}_{a_i}(t) \mathbf{S}_{a_{d_i}}(t) \mathbf{P}_{a_{d_i}}(t) + \mathbf{P}_{a_i}(t) \mathbf{S}_{a_i}(t) \mathbf{P}_{a_i}(t) = \mathbf{0} \quad (30)$$

where $\mathbf{S}_{a_i} = \mathbf{B}_{a_i} R^{-1} \mathbf{B}_{a_i}^T$ and $\mathbf{S}_{a_{d_i}} = \mathbf{B}_{a_{d_i}} R_d^{-1} \mathbf{B}_{a_{d_i}}^T$.

5. Result and Discussion

Here, the simulation results of the parameter identification and the LQIDG-Controller for the quadrotor platform are presented. First, the quadrotor parameters are estimated based on the NLS method. Then, the performance of the LQDG controller structure is evaluated. the parameters of the quadrotor and LQIR-DG are presented in Tables 1 and 2, respectively.

Table 1: Quadrotor Parameters

Parameter	Unit	Value
dcg	m	0.2
d	N.m.sec ² /rad ²	3.2×10^{-6}
b	N.sec ² /rad ²	3.13×10^{-5}
Ixx	kg.m ²	0.02839
Iyy	kg.m ²	0.03066
Izz	kg.m ²	0.0439
Irotor	kg.m ²	4.4398×10^{-5}
Ω_{mean}	rpm	3000

Table 2: LQIR-DG Controller Parameters

Channel	Weighting Matrix	Values
Roll	\mathbf{Q}_{roll}	$\text{diag}([0.02, 65.96, 83.04, 0.00])$
Pitch	$\mathbf{Q}_{\text{pitch}}$	$\text{diag}([435.01, 262.60, 262.60, 0.00])$
Yaw	\mathbf{Q}_{yaw}	$\text{diag}([4 \times 10^{-4}, 0.00, 0.133, 0])$
	R	1
	R_d	1.2764

5.1. Identification of the 3DoF quadrotor platform model

As described in section 3.3, the parameters of the quadrotor platform, denoted by $\Gamma_i (i = 1, \dots, 8)$, are identified using the NLS-TRR algorithm. To

increase accuracy of parameter identification, three scenarios are considered according to Table 3. In the first scenario, depicted in Figure 5, the quadrotor rotates about only one axis (roll, pitch, or yaw axes) to identify the parameters Γ_3 , Γ_6 , and Γ_8 . In the second scenario, according to Figure 6, the parameters Γ_2 and Γ_5 are estimated by rotating the experimental platform around its roll and pitch axes simultaneously. In the second scenario, according to Figure 6, the parameters Γ_2 and Γ_5 are estimated by rotating the experimental platform around its roll and pitch axes simultaneously. Finally, Figure 7 shows the results of the third scenario including the estimation of the parameters Γ_1 , Γ_4 , and Γ_7 of the UAV model when the platform freely rotates around three axes. When the stopping condition of the NLS algorithm is met, the optimal values of the quadrotor parameters are computed and denoted in Table 4. These results illustrate that the outputs of the simulation results for the quadrotor model are consistent with reality.

Table 3: Scenarios for Identification of Quadrotor Parameters.

Scenario	Description	Initial Condition (deg)			Rotational Velocity Commands (rpm)			
		ϕ	θ	ψ	Ω_1	Ω_2	Ω_3	Ω_4
I	roll free	38	-	-	2000	2000	2000	3400
	pitch free	-	-15	-	3700	2000	2000	2000
	yaw free	-	-	-75	2000	3300	2000	3300
II	roll & pitch free	8	-5	-	1700	3800	2400	1700
III	roll, pitch, & yaw free	8	-3	-146	1700	3800	2400	1700

Table 4: True values of the quadrotor parameters.

Parameter	Value	Parameter	Value
Γ_1	-0.9622	Γ_5	3.6441×10^{-4}
Γ_2	-0.0154	Γ_6	7.5395×10^{-5}
Γ_3	5.4716×10^{-5}	Γ_7	0.1308
Γ_4	1.0457	Γ_8	4.3753×10^{-5}

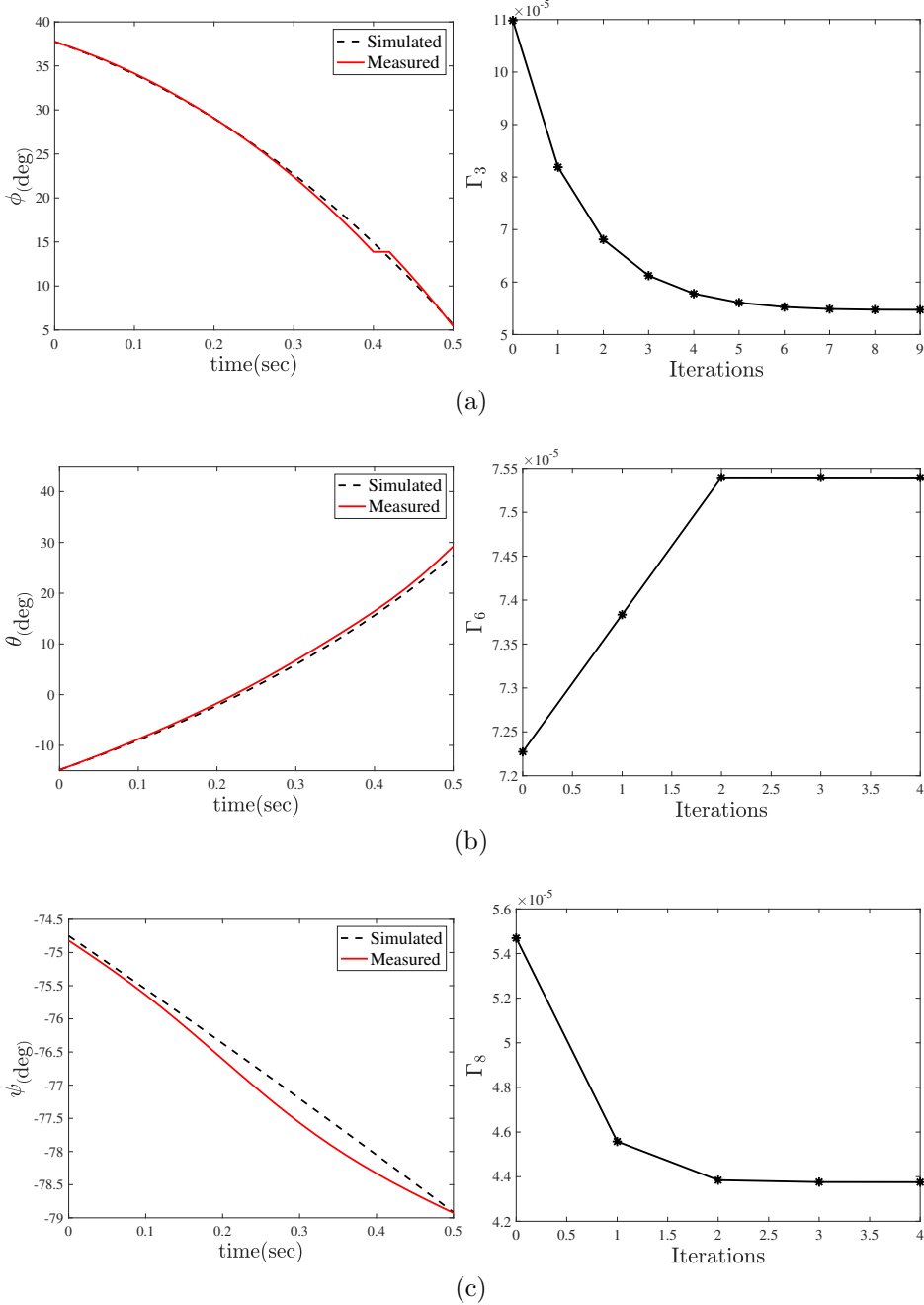


Figure 5: Identification process results when the quadrotor rotates about only one axis:
 (a) Identification of Γ_3 in free roll motion. (b) Identification of Γ_6 in free pitch motion.
 (c) Identification of Γ_8 in free yaw motion.

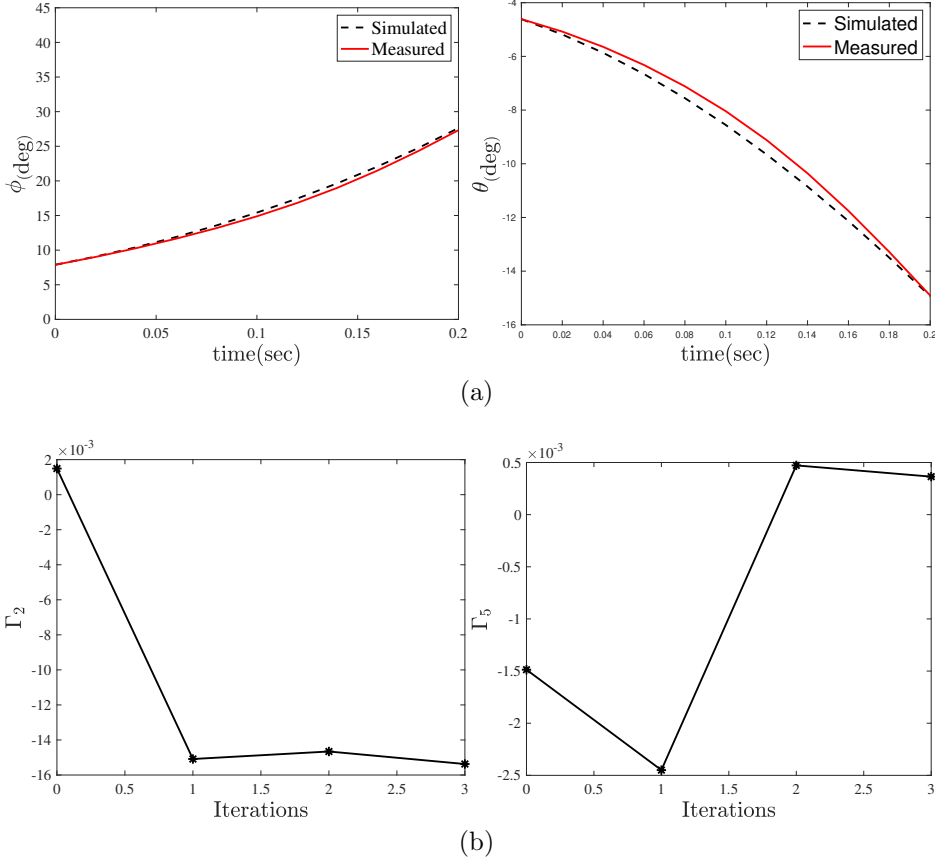


Figure 6: Identification process results when the quadrotor rotates about its roll and pitch axes: (a) Comparison of Simulation and experimental results. (b) Identification of Γ_2 and Γ_5 .

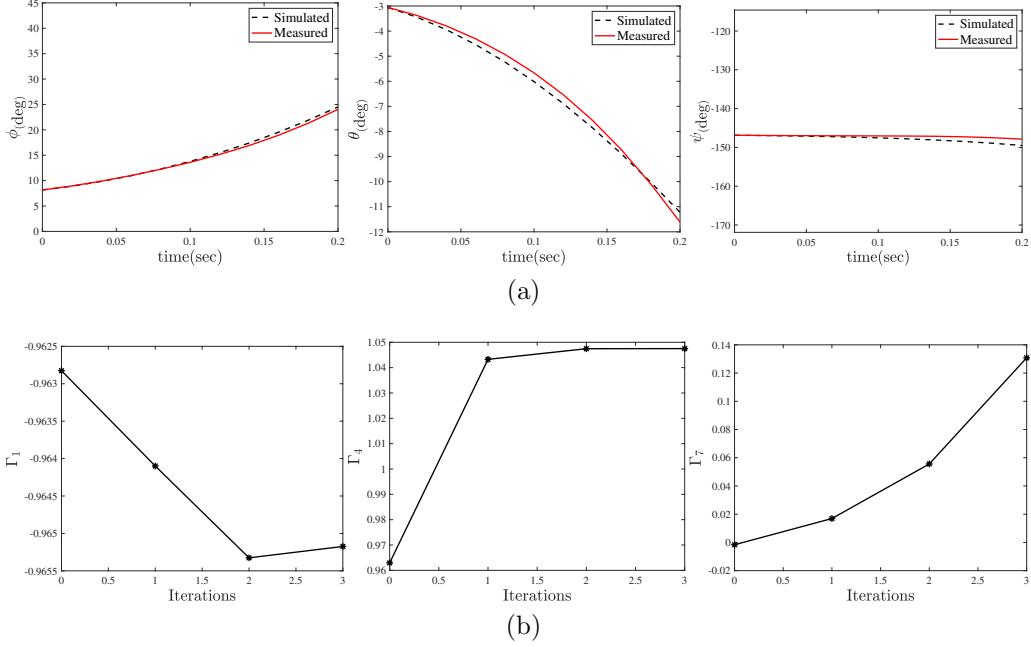


Figure 7: Identification process results when the quadrotor rotates about its roll, pitch, and yaw axes: (a) Comparison of Simulation and experimental results. (b) Identification of Γ_1^{-1} , Γ_4 and Γ_7 parameters.

5.2. Evaluation of LQIR-DG Performance

In this section the LQIR-DG controller algorithm is evaluated in three scenarios I) regulation and tracking problem, II) disturbance rejection, and III) the impact of model uncertainty. Finally, a comparison of the proposed controller is performed with a PID controller and variants of the LQR controller. PID controller parameters are presented in Table 5.

Table 5: PID Controller Parameters

Channel	K_p	K_i	K_d
roll	18	6	9
pitch	22	15	16

5.2.1. Performance of the LQIR-DG Controller

The results of the proposed approach are presented for tracking the desired roll and pitch angles of the experimental platform in Figures 8 and 9. Figure 8 (a) compares the desired and output signals, i.e., the euler angles during regulation problem. Moreover, Figure 8 (b) compares the desired square wave input with a frequency of 0.02 Hz and an amplitude of 20 degrees with the output signals when the quadrotor platform freely rotates around roll and pitch simultaneity. Figures 9 (a) and (b) show the rotational velocity command of the quadrotor in the regulation and tracking problems, respectively. These results demonstrate that the roll and pitch angles are accurately controlled by the proposed approach.

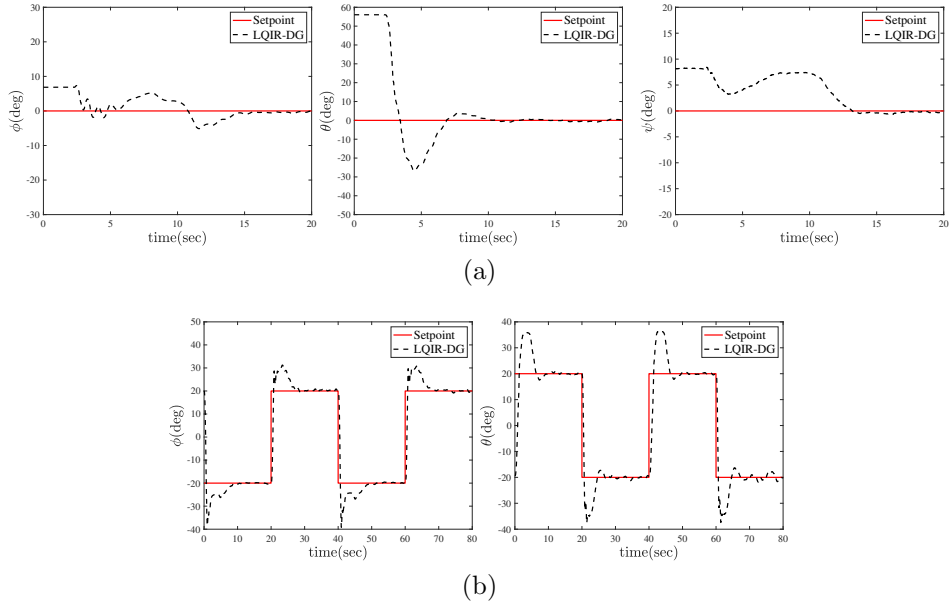


Figure 8: Comparison of Roll and Pitch Angles in (a) Regulation (b) Tracking Problem.

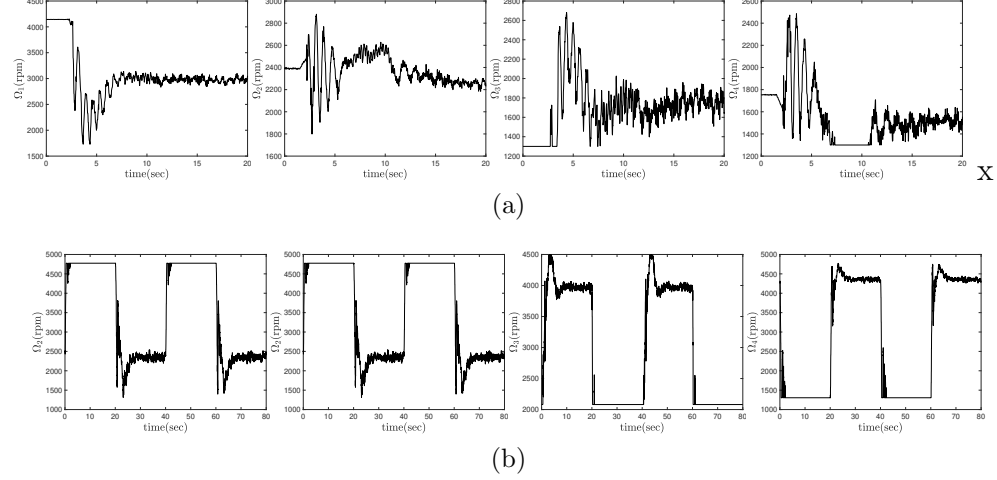


Figure 9: Rotational Velocity Commands in (a) Regulation (b) Tracking Problems.

5.2.2. Performance of the LQIR-DG in Disturbance Rejection

The performance of the proposed controller with the input disturbance is shown in Figure 10. The input disturbance, d_{Ω_i} , is considered as a change in the command of the rotational velocity, modeled as

$$d_{\Omega_1} = d_{\Omega_2} = -d_{\Omega_3} = -d_{\Omega_4} = \begin{cases} 500_{\text{rpm}} & 20 < t < 60 \\ 0 & \text{otherwise} \end{cases} \quad (31)$$

Figure 10 illustrates the roll and pitch angles in the regulation problem when the input disturbance occurs. The results indicate that the LQIR-DG controller can stabilize the quadrotor platform when the input disturbance is present.

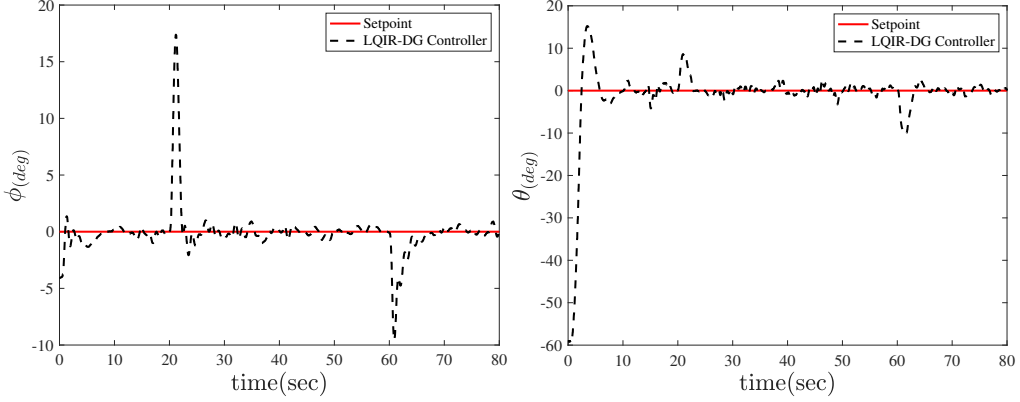


Figure 10: Comparison of the Desired and Actual Roll and Pitch Angles when the Input Disturbance Occurs.

5.2.3. Investigating the Impact of Modeling Uncertainty

Here the performance of the LQIR-DG controller is evaluated when the uncertainty is considered 3DoF experimental model. To achieve this, 50 and 100 grams weights are added to the roll and pitch axes, respectively, as shown in Figure 11. Figure 12 (a) compares the desired and the actual roll angle and Figure 12 (b) shows the desired and the actual pitch angle when the uncertainty of moments of inertia is present. Moreover, Figure 12 (c) shows the rotational velocity command of the experimental platform in the presence of model uncertainty. The implementation results indicate that the LQIR-DG controller converges to the desired values in the presence of the modeling uncertainty.

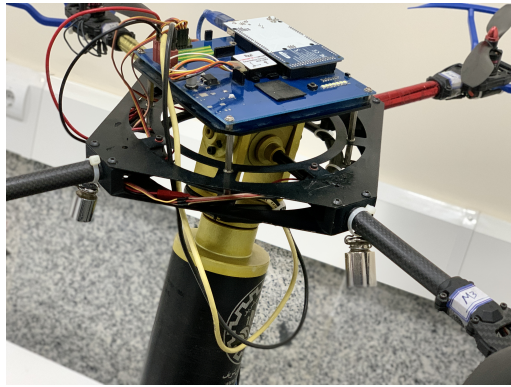


Figure 11: Quadrotor 3DoF Platform with Added Weights.

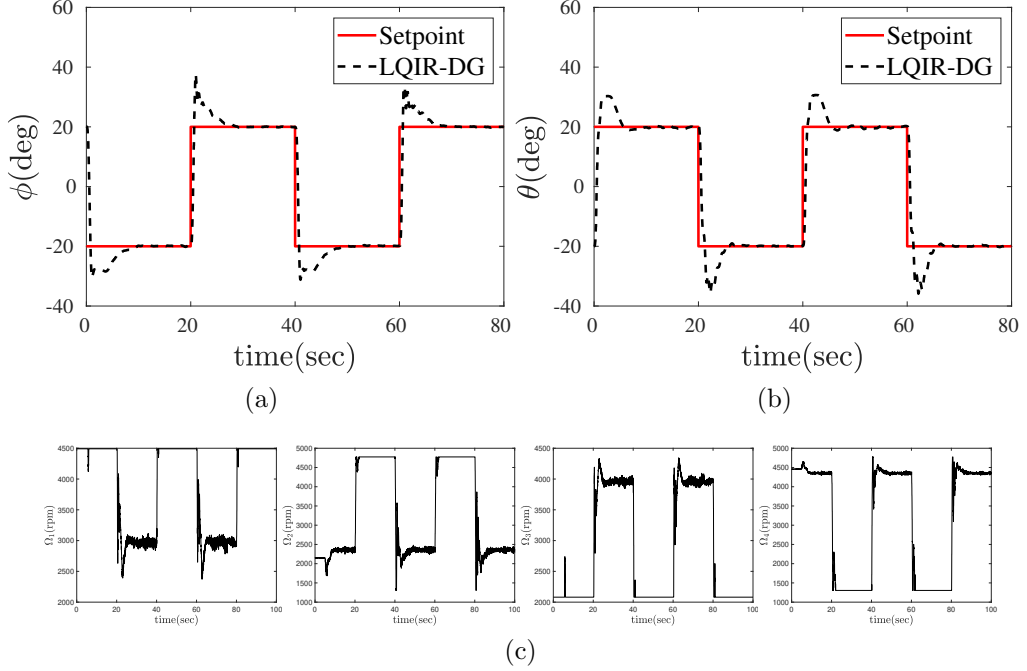


Figure 12: Comparison of the LQIR-DG Controller when the Uncertainty of Moment of Inertia is Present.

5.2.4. Comparison with the Control Strategies

Figure 13 compare, the LQIR-DG controller performance with the PID controller and variant of the LQR strategies such as the LQR and LQIR. Figure 13 compare the desired and the actual attitude of the quadrotor platform in the presence of these controllers. Moreover, the box plot of all controllers based on cost function (24), is shown in Figure 14. The median of RMSE is shown in the crossline in the box plot.

These results indicate that the LQIR-DG controller is able to provide an excellent transient response and rapid convergence relative to other controllers for attitude control of the experimental platform.

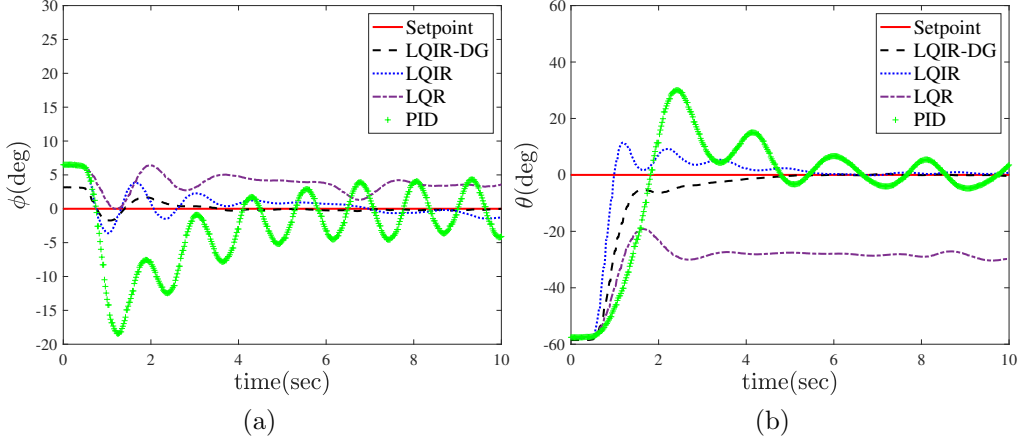


Figure 13: Comparison of LQIR-DG Controller to the LQR, LQIR, and PID in Control of the Quadrotor Outputs: (a) Roll Angle (b) Pitch Angle.

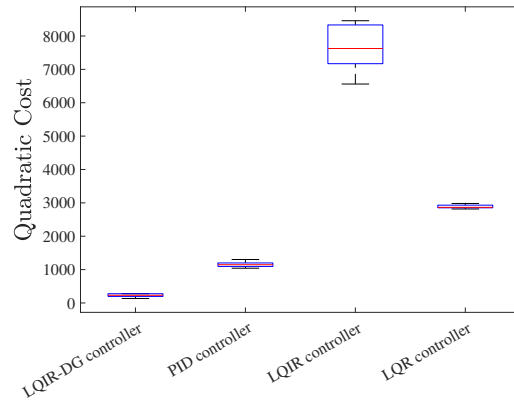


Figure 14: Box Plot of LQIR-DG, LQR, LQIR, and PID Controllers.

6. Conclusion

In this paper, the LQIR-DG method, which is an optimal controller based on the game theory, was used in real-time for attitude control of platform quadrotor. To implement the proposed controller, an accurate dynamic model was considered for the experimental platform. Then, the model parameters were identified using the NSL method. For evaluation of the proposed method, the purpose of regulation and tracking problems was successfully performed. Moreover, the ability of the proposed method was investigated for

to rejection of the input disturbance and modeling error in the laboratory experiment. The implementation results illustrated the successful performance of the proposed method in attitude control for the quadratic platform.

References

- Bouabdallah, S., 2007. Design and control of quadrotors with application to autonomous flying doi:10.5075/epfl-thesis-3727.
- Bouabdallah, S., Siegwart, R., 2007. Full control of a quadrotor, in: 2007 IEEE/RSJ International Conference on Intelligent Robots and Systems, pp. 153–158. doi:10.1109/IROS.2007.4399042.
- Engwerda, J., 2006. Linear Quadratic Games: An Overview. WorkingPaper. Macroeconomics. Subsequently published in Advances in Dynamic Games and their Applications (book), 2009 Pagination: 32.